Photothermal studies of single molecules and gold nanoparticles : vapor nanobubbles and conjugated polymers

Hou, L.

Bibliography

[1] H. Stanley. *Introduction to Phase Transitions and Critical Phenomena*. Oxford University Press, 1971.

[2] Wikipedia. Phase diagram, 2015.

[3] C. Brennen. *Cavitation and Bubble Dynamics*. Oxford University Press, New York, 1995.

[4] W. Lauterborn and T. Kurz. Physics of bubble oscillations. *Reports on Progress in Physics*, 73:106501, 2010.

[5] M. P. Brenner, S. Hilgenfeldt, and D. Lohse. Single-bubble sonoluminescence. *Reviews of Modern Physics*, 74(2):425–484, 2002.

[6] D. Lapotko. Plasmonic nanoparticle-generated photothermal bubbles and their biomedical applications. *Nanomedicine*, 4(7):813–845, 2009.

[7] Y. Wang, X. Li, Y. Zhou, P. Huang, and Y. Xu. Preparation of nanobubbles for ultrasound imaging and intracelluar drug delivery. *International Journal of Pharmaceutics*, 384(1-2):148–153, 2010.

[8] E. Boulais, R. Lachaine, A. Hatef, and M. Meunier. Plasmonics for pulsed-laser cell nanosurgery: Fundamentals and applications. *Journal of Photochemistry and Photobiology C: Photochemistry Reviews*, 17:26–49, 2013.

[9] E. Y. Lukianova-Hleb, K. M. Campbell, P. E. Constantinou, J. Braam, J. S. Olson, R. E. Ware, J. Sullivan, D. J., and D. O. Lapotko. Hemozoin-generated vapor nanobubbles for transdermal reagent- and needle-free detection of malaria. *Proceedings of the National Academy of Sciences of the United States of America*, 111(3):900–905, 2014.

[10] A. S. Goy and J. W. Fleischer. Resolution enhancement in nonlinear photoacoustic imaging. *Applied Physics Letters*, 107(21):211102, 2015.

[11] J. R. Adleman, D. A. Boyd, D. G. Goodwin, and D. Psaltis. Heterogenous catalysis mediated by plasmon heating. *Nano Letters*, 9(12):4417–4423, 2009.

[12] M. Blander and J. L. Katz. Bubble nucleation in liquids. *American Institute of Chemical Engineers Journal*, 21(5):833–848, 1975.

[13] E. Lukianova-Hleb, Y. Hu, L. Latterini, L. Tarpani, S. Lee, R. A. Drezek, J. H. Hafner, and D. O. Lapotko. Plasmonic nanobubbles as transient vapor nanobubbles generated around plasmonic nanoparticles. *ACS Nano*, 4(4):2109–2123, 2010.

[14] O. M. F. R. S. Lord Rayleigh. On the pressure developed in a liquid during the collapse of a spherical cavity. *Philosophical Magazine Series 6*, 34(200):94–98, 1917.

[15] M. S. Plesset and A. Prosperetti. Bubble dynamics and cavitation. *Annual Review of Fluid Mechanics*, 9:145–185, 1977.

[16] J. Lombard, T. Biben, and S. Merabia. Kinetics of nanobubble generation around overheated nanoparticles. *Physical Review Letters*, 112(10):105701, 2014.

[17] M. Minnaert. On musical air-bubbles and the sounds of running water. *The London, Edinburgh, and Dublin Philosophical Magazine and Journal of Science*, 16(104):235–248, 1933.

[18] L. Stricker, B. Dollet, D. Fernández Rivas, and D. Lohse. Interacting bubble clouds and their sonochemical production. *The Journal of the Acoustical Society of America*, 134(3):1854–1862, 2013.

[19] F. Gilmore. The growth or collapse of a spherical bubble in a viscous compressible liquid. Report, Hydrodynamics Laboratory, California Institute of Technology, 1952.

[20] K. de Graaf, I. Penesis, and P. Brandner. Comparison of the Rayleigh-Plesset and Gilmore equations and additional aspects for the modelling of seismic airgun bubble dynamics. In *18th Australasian Fluid Mechanics Conference*. Leishman Associates, 2012.

[21] G. Ahlers, S. Grossmann, and D. Lohse. Heat transfer and large scale dynamics in turbulent Rayleigh-Bénard convection. *Reviews of Modern Physics*, 81(2):503–537, 2009.

[22] D. Lohse and X. Zhang. Surface nanobubbles and nanodroplets. *Reviews of Modern Physics*, 87(3):981–1035, 2015.

[23] G. Nagayama, T. Tsuruta, and P. Cheng. Molecular dynamics simulation on bubble formation in a nanochannel. *International Journal of Heat and Mass Transfer*, 49(23-24):4437–4443, 2006.

[24] M. de Saint Victor, C. Crake, C. C. Coussios, and E. Stride. Properties, characteristics and applications of microbubbles for sonothrombolysis. *Expert Opinion on Drug Delivery*, 11(2):187–209, 2014.

[25] E. Y. Lukianova-Hleb and D. O. Lapotko. Experimental techniques for imaging and measuring transient vapor nanobubbles. *Applied Physics Letters*, 101(26):264102, 2012.

[26] V. Kotaidis, C. Dahmen, G. von Plessen, F. Springer, and A. Plech. Excitation of nanoscale vapor bubbles at the surface of gold nanoparticles in water. *The Journal of Chemical Physics*, 124(18):184702, 2006.

[27] B. H. T. Goh, Y. D. A. Oh, E. Klaseboer, S. W. Ohl, and B. C. Khoo. A low-voltage spark-discharge method for generation of consistent oscillating bubbles. *Review of Scientific Instruments*, 84(1):014705, 2013.

[28] G. Nagashima, E. V. Levine, D. P. Hoogerheide, M. M. Burns, and J. A. Golovchenko. Superheating and homogeneous single bubble nucleation in a solid-state nanopore. *Physical Review Letters*, 113(2):024506, 2014.

[29] R. Lachaine, E. Boulais, and M. Meunier. From thermo- to plasma-mediated ultrafast laser-induced plasmonic nanobubbles. *ACS Photonics*, 1(4):331–336, 2014.

[30] L. Hou, M. Yorulmaz, N. R. Verhart, and M. Orrit. Explosive formation and dynamics of vapor nanobubbles around a continuously heated gold nanosphere. *New Journal of Physics*, 17(1):013050, 2015.

[31] E. Y. Lukianova-Hleb and D. O. Lapotko. Influence of transient environmental photothermal effects on optical scattering by gold nanoparticles. *Nano Letters*, 9(5):2160–2166, 2009.

[32] A. Siems, S. A. L. Weber, J. Boneberg, and A. Plech. Thermodynamics of nanosecond nanobubble formation at laser-excited metal nanoparticles. *New Journal of Physics*, 13:043018, 2011.

[33] E. V. Shashkov, M. Everts, E. I. Galanzha, and V. P. Zharov. Quantum dots as multimodal photoacoustic and photothermal contrast agents. *Nano Letters*, 8(11):3953–3958, 2008.

[34] M. T. Carlson, A. J. Green, and H. H. Richardson. Superheating water by CW excitation of gold nanodots. *Nano Letters*, 12(3):1534–1537, 2012.

[35] O. Neumann, A. S. Urban, J. Day, S. Lal, P. Nordlander, and N. J. Halas. Solar vapor generation enabled by nanoparticles. *ACS Nano*, 7(1):42–49, 2012.

[36] J. P. Padilla-Martinez, C. Berrospe-Rodriguez, G. Aguilar, J. C. Ramirez-San-Juan, and R. Ramos-Garcia. Optic cavitation with CW lasers: A review. *Physics of Fluids*, 26(12):122007, 2014.

[37] G. Baffou and H. Rigneault. Femtosecond-pulsed optical heating of gold nanoparticles. *Physical Review B*, 84(3):035415, 2011.

[38] C. U. Chan and C.-D. Ohl. Total-internal-reflection-fluorescence microscopy for the study of nanobubble dynamics. *Physical Review Letters*, 109(17):174501, 2012.

[39] Z. Fang, Y.-R. Zhen, O. Neumann, A. Polman, F. Javier Garcia de Abajo, P. Nordlander, and N. J. Halas. Evolution of light-induced vapor generation at a liquid-immersed metallic nanoparticle. *Nano Letters*, 13(4):1736–1742, 2013.

[40] E. S. Bialkowski. *Photothermal Spectroscopy Methods for Chemical Analysis*, volume 134. John Wiley and Sons, Inc, 1996.

[41] M. Selmke, M. Braun, and F. Cichos. Photothermal single-particle microscopy: Detection of a nanolens. *ACS Nano*, 6(3):2741–2749, 2012.

[42] A. Gaiduk, P. V. Ruijgrok, M. Yorulmaz, and M. Orrit. Detection limits in photothermal microscopy. *Chemical Science*, 1(3):343–350, 2010.

[43] S. Berciaud, L. Cognet, G. A. Blab, and B. Lounis. Photothermal heterodyne imaging of individual nonfluorescent nanoclusters and nanocrystals. *Physical Review Letters*, 93(25):257402, 2004.

[44] D. Boyer, P. Tamarat, A. Maali, B. Lounis, and M. Orrit. Photothermal imaging of nanometer-sized metal particles among scatterers. *Science*, 297(5584):1160–1163, 2002.

[45] A. Gaiduk, M. Yorulmaz, P. V. Ruijgrok, and M. Orrit. Room-temperature detection of a single molecule's absorption by photothermal contrast. *Science*, 330(6002):353–356, 2010.

[46] A. Arbouet, C. Voisin, D. Christofilos, P. Langot, N. D. Fatti, F. Vallée, J. Lermé, G. Celep, E. Cottancin, M. Gaudry, M. Pellarin, M. Broyer, M. Maillard, M. P. Pileni, and M. Treguer. Electron-phonon scattering in metal clusters. *Physical Review Letters*, 90(17):177401, 2003.

[47] K. Lindfors, T. Kalkbrenner, P. Stoller, and V. Sandoghdar. Detection and spectroscopy of gold nanoparticles using supercontinuum white light confocal microscopy. *Physical Review Letters*, 93(3):037401, 2004.

[48] M. A. v. Dijk. *Nonlinear optical studies of single gold nanoparticles*. Thesis, Leiden University, 2007.

[49] S. Berciaud, D. Lasne, G. A. Blab, L. Cognet, and B. Lounis. Photothermal heterodyne imaging of individual metallic nanoparticles: Theory versus experiment. *Physical Review B*, 73(4):045424, 2006.

[50] F. V. Ignatovich and L. Novotny. Real-time and background-free detection of nanoscale particles. *Physical Review Letters*, 96(1):013901, 2006.

[51] M. A. van Dijk, M. Lippitz, D. Stolwijk, and M. Orrit. A common-path interferometer for time-resolved and shot-noise-limited detection of single nanoparticles. *Optics Express*, 15(5):2273–2287, 2007.

[52] B. Simons. Phase transitions and collective phenomena, 2011. Lecture notes. http://www.tcm.phy.cam.ac.uk/ bds10/phase.html.

[53] Wikipedia. Supercritical fluid, 2016.

[54] E. C. Dreaden, A. M. Alkilany, X. Huang, C. J. Murphy, and M. A. El-Sayed. The golden age: gold nanoparticles for biomedicine. *Chemical Society Reviews*, 41(7):2740–2779, 2012.

[55] A. O. Govorov and H. H. Richardson. Generating heat with metal nanoparticles. *Nano Today*, 2(1):30–38, 2007.

[56] G. Lu, L. Hou, T. Zhang, J. Liu, H. Shen, C. Luo, and Q. Gong. Plasmonic sensing via photoluminescence of individual gold nanorod. *The Journal of Physical Chemistry C*, 116(48):25509–25516, 2012.

[57] Q. Wang, G. Lu, L. Hou, T. Zhang, C. Luo, H. Yang, G. Barbillon, F. H. Lei, C. A. Marquette, P. Perriat, O. Tillement, S. Roux, Q. Ouyang, and Q. Gong. Fluorescence correlation spectroscopy near individual gold nanoparticle. *Chemical Physics Letters*, 503(4-6):256–261, 2011.

[58] P. Zijlstra, P. M. R. Paulo, and M. Orrit. Optical detection of single non-absorbing molecules using the surface plasmon resonance of a gold nanorod. *Nature Nanotechnology*, 7(6):379–382, 2012.

[59] H. Yuan, S. Khatua, P. Zijlstra, M. Yorulmaz, and M. Orrit. Thousand-fold enhancement of single-molecule fluorescence near a single gold nanorod. *Angewandte Chemie International Edition*, 52(4):1217–1221, 2013.

[60] J. H. Burroughes, D. D. C. Bradley, A. R. Brown, R. N. Marks, K. Mackay, R. H. Friend, P. L. Burns, and A. B. Holmes. Light-emitting diodes based on conjugated polymers. *Nature*, 347(6293):539–541, 1990.

[61] S. Günes, H. Neugebauer, and N. S. Sariciftci. Conjugated polymer-based organic solar cells. *Chemical Reviews*, 107(4):1324–1338, 2007.

[62] M. Vacha and S. Habuchi. Conformation and physics of polymer chains: a single-molecule perspective. *NPG Asia Materials*, 2:134–142, 2010.

[63] D. Hu, J. Yu, and P. F. Barbara. Single-molecule spectroscopy of the conjugated polymer MEH-PPV. *Journal of the American Chemical Society*, 121(29):6936–6937, 1999.

[64] P. Debenedetti. *Metastable Liquids: Concepts and Principles*. Princeton University Press, 1996.

[65] P. J. Linstrom and W. G. Mallard. National Institute of Standards and Technology (NIST) Chemistry WebBook, NIST Standard Reference Database Number 69, 2011. http://webbook.nist.gov/chemistry/.

[66] S. Merabia, P. Keblinski, L. Joly, L. Lewis, and J.-L. Barrat. Critical heat flux around strongly heated nanoparticles. *Physical Review E*, 79(2):021404, 2009.

[67] H. Carslaw and J. Jaeger. *Conduction of Heat in Solids*. Clarendon Press, 1986.

[68] Wikipedia. Knudsen number, 2016.

[69] K. Yang, Y. Zhou, Q. Ren, J. Y. Ye, and C. X. Deng. Dynamics of microbubble generation and trapping by self-focused femtosecond laser pulses. *Applied Physics Letters*, 95(5):051107, 2009.

[70] A. Vogel, N. Linz, and S. Freidank. Femtosecond-laser-induced nanocavitation in water: implications for optical breakdown threshold and cell surgery. *Physical Review Letters*, 100(3):038102, 2008.

[71] V. Kotaidis and A. Plech. Cavitation dynamics on the nanoscale. *Applied Physics Letters*, 87(21):213102, 2005.

[72] V. Zharov and D. Lapotko. Photothermal sensing of nanoscale targets. *Review of Scientific Instruments*, 74(1):785–788, 2003.

[73] E. Boulais, R. Lachaine, and M. Meunier. Plasma mediated off-resonance plasmonic enhanced ultrafast laser-induced nanocavitation. *Nano Letters*, 12(9):4763–4769, 2012.

[74] T. Katayama, K. Setoura, D. Werner, H. Miyasaka, and S. Hashimoto. Picosecond-to-nanosecond dynamics of plasmonic nanobubbles from pump-probe spectral measurements of aqueous colloidal gold nanoparticles. *Langmuir*, 30(31):9504–9513, 2014.

[75] G. Baffou, J. Polleux, H. Rigneault, and S. Monneret. Super-heating and micro-bubble generation around plasmonic nanoparticles under cw illumination. *The Journal of Physical Chemistry C*, 118(9):4890–4898, 2014.

[76] A. Heber, M. Selmke, and F. Cichos. Metal nanoparticle based all-optical photothermal light modulator. *ACS Nano*, 8(2):1893–1898, 2014.

[77] X. Zhang, D. Y. C. Chan, D. Wang, and N. Maeda. Stability of interfacial nanobubbles. *Langmuir*, 29(4):1017–1023, 2012.

[78] X. Zhang, H. Lhuissier, C. Sun, and D. Lohse. Surface nanobubbles nucleate microdroplets. *Physical Review Letters*, 112(14):144503, 2014.

[79] E. Y. Lukianova-Hleb, X. Ren, R. R. Sawant, X. Wu, V. P. Torchilin, and D. O. Lapotko. On-demand intracellular amplification of chemoradiation with cancer-specific plasmonic nanobubbles. *Nature Medicine*, 20(7):778–784, 2014.

[80] J. Yao, L. Wang, C. Li, C. Zhang, and L. V. Wang. Photoimprint photoacoustic microscopy for three-dimensional label-free subdiffraction imaging. *Physical Review Letters*, 112(1):014302, 2014.

[81] A. Gaiduk, M. Yorulmaz, and M. Orrit. Correlated absorption and photoluminescence of single gold nanoparticles. *ChemPhysChem*, 12(8):1536–1541, 2011.

[82] P. Zijlstra and M. Orrit. Single metal nanoparticles: optical detection, spectroscopy and applications. *Reports on Progress in Physics*, 74(10):106401, 2011.

[83] P. V. Ruijgrok, N. R. Verhart, P. Zijlstra, A. L. Tchebotareva, and M. Orrit. Brownian fluctuations and heating of an optically aligned gold nanorod. *Physical Review Letters*, 107(3):037401, 2011.

[84] I. U. Vakarelski, N. A. Patankar, J. O. Marston, D. Y. C. Chan, and S. T. Thoroddsen. Stabilization of Leidenfrost vapour layer by textured superhydrophobic surfaces. *Nature*, 489(7415):274–277, 2012.

[85] B. Gompf and R. Pecha. Mie scattering from a sonoluminescing bubble with high spatial and temporal resolution. *Physical Review E*, 61(5):5253–5256, 2000.

[86] R. G. Holt, D. F. Gaitan, A. A. Atchley, and J. Holzfuss. Chaotic sonoluminescence. *Physical Review Letters*, 72(9):1376–1379, 1994.

[87] D. Lide. *CRC Handbook of Chemistry and Physics (Internet Version 2005)*. CRC Press, Boca Raton, FL, 2005.

[88] The triisopropylbenzene is the main component of oil, sound velocities in some related compounds is about 1350 m/s, data from a commercial website (https://www.flexim.com).

[89] E. Y. Lukianova-Hleb, Y.-S. Kim, I. Belatsarkouski, A. M. Gillenwater, B. E. O'Neill, and D. O. Lapotko. Intraoperative diagnostics and elimination of residual microtumours with plasmonic nanobubbles. *Nature Nanotechnology*, advance online publication, 2016.

[90] D. A. Boyd, L. Greengard, M. Brongersma, M. Y. El-Naggar, and D. G. Goodwin. Plasmon-assisted chemical vapor deposition. *Nano Letters*, 6(11):2592–2597, 2006.

[91] H. H. Richardson, M. T. Carlson, P. J. Tandler, P. Hernandez, and A. O. Govorov. Experimental and theoretical studies of light-to-heat conversion and collective heating effects in metal nanoparticle solutions. *Nano Letters*, 9(3):1139–1146, 2009.

[92] S. Hashimoto, D. Werner, and T. Uwada. Studies on the interaction of pulsed lasers with plasmonic gold nanoparticles toward light manipulation, heat management, and nanofabrication. *Journal of Photochemistry and Photobiology C: Photochemistry Reviews*, 13(1):28–54, 2012.

[93] D. Lapotko. Optical excitation and detection of vapor bubbles around plasmonic nanoparticles. *Optics Express*, 17(4):2538–2556, 2009.

[94] A. Plech, V. Kotaidis, M. Lorenc, and M. Wulff. Thermal dynamics in laser excited metal nanoparticles. *Chemical Physics Letters*, 401(4-6):565–569, 2005.

[95] P. V. Ruijgrok, P. Zijlstra, A. L. Tchebotareva, and M. Orrit. Damping of acoustic vibrations of single gold nanoparticles optically trapped in water. *Nano Letters*, 12(2):1063–9, 2012.

[96] D. Werner and S. Hashimoto. Improved working model for interpreting the excitation wavelength- and fluence-dependent response in pulsed laser-induced size reduction of aqueous gold nanoparticles. *The Journal of Physical Chemistry C*, 115(12):5063–5072, 2011.

[97] Z. Lin, L. V. Zhigilei, and V. Celli. Electron-phonon coupling and electron heat capacity of metals under conditions of strong electron-phonon nonequilibrium. *Physical Review B*, 77(7):075133, 2008.

[98] M. Strasser, K. Setoura, U. Langbein, and S. Hashimoto. Computational modeling of pulsed laser-induced heating and evaporation of gold nanoparticles. *The Journal of Physical Chemistry C*, 118(44):25748–25755, 2014.

[99] A. Plech, V. Kotaidis, S. Grésillon, C. Dahmen, and G. von Plessen. Laser-induced heating and melting of gold nanoparticles studied by time-resolved X-ray scattering. *Physical Review B*, 70(19):195423, 2004.

[100] H. Lamb. On the vibrations of an elastic sphere. *Proceedings of the London Mathematical Society*, s1-13(1):189–212, 1881.

[101] C. Voisin, D. Christofilos, N. Del Fatti, and F. Vallée. Environment effect on the acoustic vibration of metal nanoparticles. *Physica B: Condensed Matter*, 316-317:89–94, 2002.

[102] K. Yu, P. Zijlstra, J. E. Sader, Q.-H. Xu, and M. Orrit. Damping of acoustic vibrations of immobilized single gold nanorods in different environments. *Nano Letters*, 13(6):2710–2716, 2013.

[103] V. Juvé, M. Scardamaglia, P. Maioli, A. Crut, S. Merabia, L. Joly, N. Del Fatti, and F. Vallée. Cooling dynamics and thermal interface resistance of glass-embedded metal nanoparticles. *Physical Review B*, 80(19):195406, 2009.

[104] O. M. Wilson, X. Hu, D. G. Cahill, and P. V. Braun. Colloidal metal particles as probes of nanoscale thermal transport in fluids. *Physical Review B*, 66(22):224301, 2002.

[105] M. Hu and G. V. Hartland. Heat dissipation for Au particles in aqueous solution: Relaxation time versus size. *The Journal of Physical Chemistry B*, 106(28):7029–7033, 2002.

[106] F. Cooper. Heat transfer from a sphere to an infinite medium. *International Journal of Heat and Mass Transfer*, 20(9):991–993, 1977.

[107] M. Hu, H. Petrova, and G. V. Hartland. Investigation of the properties of gold nanoparticles in aqueous solution at extremely high lattice temperatures. *Chemical Physics Letters*, 391(4-6):220–225, 2004.

[108] K. Setoura, D. Werner, and S. Hashimoto. Optical scattering spectral thermometry and refractometry of a single gold nanoparticle under CW laser excitation. *The Journal of Physical Chemistry C*, 116(29):15458–15466, 2012.

[109] S. Berciaud, L. Cognet, and B. Lounis. Photothermal absorption spectroscopy of individual semiconductor nanocrystals. *Nano Letters*, 5(11):2160–2163, 2005.

[110] S. Berciaud, L. Cognet, P. Poulin, R. B. Weisman, and B. Lounis. Absorption spectroscopy of individual single-walled carbon nanotubes. *Nano Letters*, 7(5):1203–1207, 2007.

[111] S. Li, L. Guo, C. Liu, and Y. Zhang. Application of supercritical fluid extraction coupled with counter-current chromatography for extraction and online isolation of unstable chemical components from rosa damascena. *Journal of Separation Science*, 36(13):2104–2113, 2013.

[112] P. M. Rentzepis and D. C. Douglass. Xenon as a solvent. *Nature*, 293(5828):165–166, 1981.

[113] D. H. Garside, H. V. Molgaard, and B. L. Smith. Refractive index and Lorentz-Lorenz function of xenon liquid and vapour. *Journal of Physics B: Atomic and Molecular Physics*, 1(3):449, 1968.

[114] R. A. Leach and J. M. Harris. Supercritical fluids as spectroscopic solvents for thermooptical absorption measurements. *Analytical Chemistry*, 56(8):1481–1487, 1984.

[115] L. Pagliaro, F. Reitz, and J. Wang. An optical pressure chamber designed for high numerical aperture studies on adherent living cells. *The Undersea and Hyperbaric Medicine*, 22(2):171–181, 1995.

[116] S. Timoshenko and S. Woinowsky-Krieger. *Theory of Plates and Shells*. McGraw-Hill College; 2 edition, New York, 1987.

[117] M. E. Briggs and R. W. Gammon. Photothermal deflection in a supercritical fluid. *International Journal of Thermophysics*, 16(6):1439–1453, 1995.

[118] D. L. Huber. Critical slowing down in an anisotropic ferromagnet. *Physics Letters A*, 28(9):644–645, 1969.

[119] D. Hu, J. Yu, K. Wong, B. Bagchi, P. J. Rossky, and P. F. Barbara. Collapse of stiff conjugated polymers with chemical defects into ordered, cylindrical conformations. *Nature*, 405(6790):1030–1033, 2000.

[120] M. Orrit and J. Bernard. Single pentacene molecules detected by fluorescence excitation in a *p* -terphenyl crystal. *Physical Review Letters*, 65(21):2716–2719, 1990.

[121] D. A. V. Bout, W.-T. Yip, D. Hu, D.-K. Fu, T. M. Swager, and P. F. Barbara. Discrete intensity jumps and intramolecular electronic energy transfer in the spectroscopy of single conjugated polymer molecules. *Science*, 277(5329):1074–1077, 1997.

[122] T. Huser, M. Yan, and L. J. Rothberg. Single chain spectroscopy of conformational dependence of conjugated polymer photophysics. *Proceedings of the National Academy of Sciences of the United States of America*, 97(21):11187–11191, 2000.

[123] K. Becker and J. M. Lupton. Efficient light harvesting in dye-endcapped conjugated polymers probed by single molecule spectroscopy. *Journal of the American Chemical Society*, 128(19):6468–6479, 2006.

[124] F. Schindler, J. M. Lupton, J. Feldmann, and U. Scherf. A universal picture of chromophores in pi-conjugated polymers derived from single-molecule spectroscopy. *Proceedings of the National Academy of Sciences of the United States of America*, 101(41):14695–14700, 2004.

[125] J. K. Grey, D. Y. Kim, B. C. Norris, W. L. Miller, and P. F. Barbara. Size-dependent spectroscopic properties of conjugated polymer nanoparticles. *The Journal of Physical Chemistry B*, 110(51):25568–25572, 2006.

[126] Y. J. Lee, D. Y. Kim, and P. F. Barbara. Effect of sample preparation and excitation conditions on the single molecule spectroscopy of conjugated polymers. *The Journal of Physical Chemistry B*, 110(20):9739–9742, 2006.

[127] Y. Ebihara and M. Vacha. Relating conformation and photophysics in single MEH-PPV chains. *The Journal of Physical Chemistry B*, 112(40):12575–12578, 2008.

[128] H. Kobayashi, S. Onda, S. Furumaki, S. Habuchi, and M. Vacha. A single-molecule approach to conformation and photophysics of conjugated polymers. *Chemical Physics Letters*, 528:1–6, 2012.

[129] J. Yu, D. Hu, and P. F. Barbara. Unmasking electronic energy transfer of conjugated polymers by suppression of O_2 quenching. *Science*, 289(5483):1327–1330, 2000.

[130] J.-J. Liang, J. D. White, Y. C. Chen, C. F. Wang, J. C. Hsiang, T. S. Lim, W. Y. Sun, J. H. Hsu, C. P. Hsu, M. Hayashi, W. S. Fann, K. Y. Peng, and S. A. Chen. Heterogeneous energy landscapes of individual luminescent conjugated polymers. *Physical Review B*, 74(8):085209, 2006.

[131] J. G. Müller, U. Lemmer, G. Raschke, M. Anni, U. Scherf, J. M. Lupton, and J. Feldmann. Linewidth-limited energy transfer in single conjugated polymer molecules. *Physical Review Letters*, 91(26):267403, 2003.

[132] H. Lin, S. R. Tabaei, D. Thomsson, O. Mirzov, P.-O. Larsson, and I. G. Scheblykin. Fluorescence blinking, exciton dynamics, and energy transfer domains in single conjugated polymer chains. *Journal of the American Chemical Society*, 130(22):7042–7051, 2008.

[133] T.-Q. Nguyen, V. Doan, and B. J. Schwartz. Conjugated polymer aggregates in solution: Control of interchain interactions. *The Journal of Chemical Physics*, 110(8):4068–4078, 1999.

[134] S. Onda, H. Kobayashi, T. Hatano, S. Furumaki, S. Habuchi, and M. Vacha. Complete suppression of blinking and reduced photobleaching in single MEH-PPV chains in solution. *The Journal of Physical Chemistry Letters*, 2(21):2827–2831, 2011.

[135] D. Wang, Y. Yuan, Y. Mardiyati, C. Bubeck, and K. Koynov. From single chains to aggregates, how conjugated polymers behave in dilute solutions. *Macromolecules*, 46(15):6217–6224, 2013.

[136] J. Yu, R. Lammi, A. J. Gesquiere, and P. F. Barbara. Singlet-triplet and triplet-triplet interactions in conjugated polymer single molecules. *The Journal of Physical Chemistry B*, 109(20):10025–10034, 2005.

[137] Y. Ebihara and M. Vacha. A method for determining the absorption ellipsoid of single conjugated polymer molecules and single luminescent nanoparticles. *The Journal of Chemical Physics*, 123(24):244710, 2005.

[138] K.-i. Shinohara, T. Kitami, and K. Nakamae. Direct measurement of structural diversity in single molecules of a chiral helical π-conjugated polymer. *Journal of Polymer Science Part A: Polymer Chemistry*, 42(16):3930–3935, 2004.

[139] Y. Tian, M. V. Kuzimenkova, J. Halle, M. Wojdyr, A. Diaz de Zerio Mendaza, P.-O. Larsson, C. Müller, and I. G. Scheblykin. Molecular weight determination by counting molecules. *The Journal of Physical Chemistry Letters*, 6(6):923–927, 2015.

[140] O. Mirzov and I. G. Scheblykin. Photoluminescence spectra of a conjugated polymer: from films and solutions to single molecules. *Physical Chemistry Chemical Physics*, 8(47):5569–5576, 2006.

[141] A. Gaiduk, M. Yorulmaz, E. Ishow, and M. Orrit. Absorption, luminescence, and sizing of organic dye nanoparticles and of patterns formed upon dewetting. *ChemPhysChem*, 13(4):946–951, 2012.

[142] N. C. Greenham, I. D. W. Samuel, G. R. Hayes, R. T. Phillips, Y. A. R. R. Kessener, S. C. Moratti, A. B. Holmes, and R. H. Friend. Measurement of absolute photoluminescence quantum efficiencies in conjugated polymers. *Chemical Physics Letters*, 241(1-2):89–96, 1995.

[143] H. Lin, Y. Tian, K. Zapadka, G. Persson, D. Thomsson, O. Mirzov, P.-O. Larsson, J. Widengren, and I. G. Scheblykin. Fate of excitations in conjugated polymers: Single-molecule spectroscopy reveals nonemissive "dark" regions in MEH-PPV individual chains. *Nano Letters*, 9(12):4456–4461, 2009.

[144] E. N. Hooley, A. J. Tilley, J. M. White, K. P. Ghiggino, and T. D. M. Bell. Energy transfer in PPV-based conjugated polymers: a defocused widefield fluorescence microscopy study. *Physical Chemistry Chemical Physics*, 16(15):7108–7114, 2014.

Appendices

A

Thermodynamic and optical data of some common substances

Table A.1: Thermodynamic and optical data of some common substances at ambient temperature and pressure*

Substance	n	$10^4 \times \frac{\partial n}{\partial T}$ (K^{-1})	ρ ($g \cdot cm^{-3}$)	κ ($Wm^{-1}K^{-1}$)	$10^{-3} \times C_p$ ($Jkg^{-1}K^{-1}$)	$10^3 \times \gamma$ ($N \cdot m^{-1}$)	$10^3 \times \mu$ ($Pa \cdot s$)	$T_b(T_m)$ (C°)	v_l ($m \cdot s^{-1}$)	v_s ($m \cdot s^{-1}$)
water(25 $C°$)	1.33	-0.91	0.997	0.61	4.18	71.99	0.89	100	1497	-
glycerol	1.47	-2.7	1.261	0.28	2.4	63	1495	290	1904	-
n-pentane	1.36	-5.5	0.626	0.11	2.31	15.49	0.22	36.1	1008	-
methanol	1.31	-3.94	0.792	0.202	2.46	22.07	0.59	64.6	1121	-
ethanol	1.36	-3.7	0.789	0.167	2.36	21.97	1.203	78.2	1162	-
toluene	1.50	-5.68	0.87	0.135	1.69	27.73	0.56	110.6	1304	-
acetone	1.36	-5.42	0.8	0.19	2.18	22.72	0.295	56	1203	-
BK7 glass	1.52	-0.13	2.51	1.114	0.86	-	-	557	5100	2840
SiO_2	1.46	-0.12	2.2	1.38	0.703	-	-	1600	5968	3764
gold	0.27+2.95i	unknown	19.3	318	0.129	-	-	1064	3240	1200
PMMA	1.49	-1.2	1.19	0.17-0.19	1.4-1.5	-	-	160	unknown	unknown
air	1	-0.01	0.001	0.026	1.01	-	0.018	-	346	-
water steam (100 $C°$)	1	unknown	0.001	0.025	2.08	-	0.012	-	472	-

(*The tabulated constants for each material are the refractive index n at 589.3 nm, the derivative of refractive index with respect to temperature $\frac{\partial n}{\partial T}$, the density ρ, the thermal conductivity κ, the heat capacity C_p, the surface tension (of liquid) γ, the viscosity μ, the boiling point T_b for liquids, the melting point T_m for solids, the velocity of longitudinal sound waves v_l, and the velocity of shear waves v_s. The data are from the CRC Handbook of Chemistry and Physics (90^{th}), National Institute of Standards and Technology (NIST), and Photothermal Spectroscopy Methods for Chemical Analysis [40]. The "unknown" means the data are not found in the above resources.)

B

Scheme of the pressure system

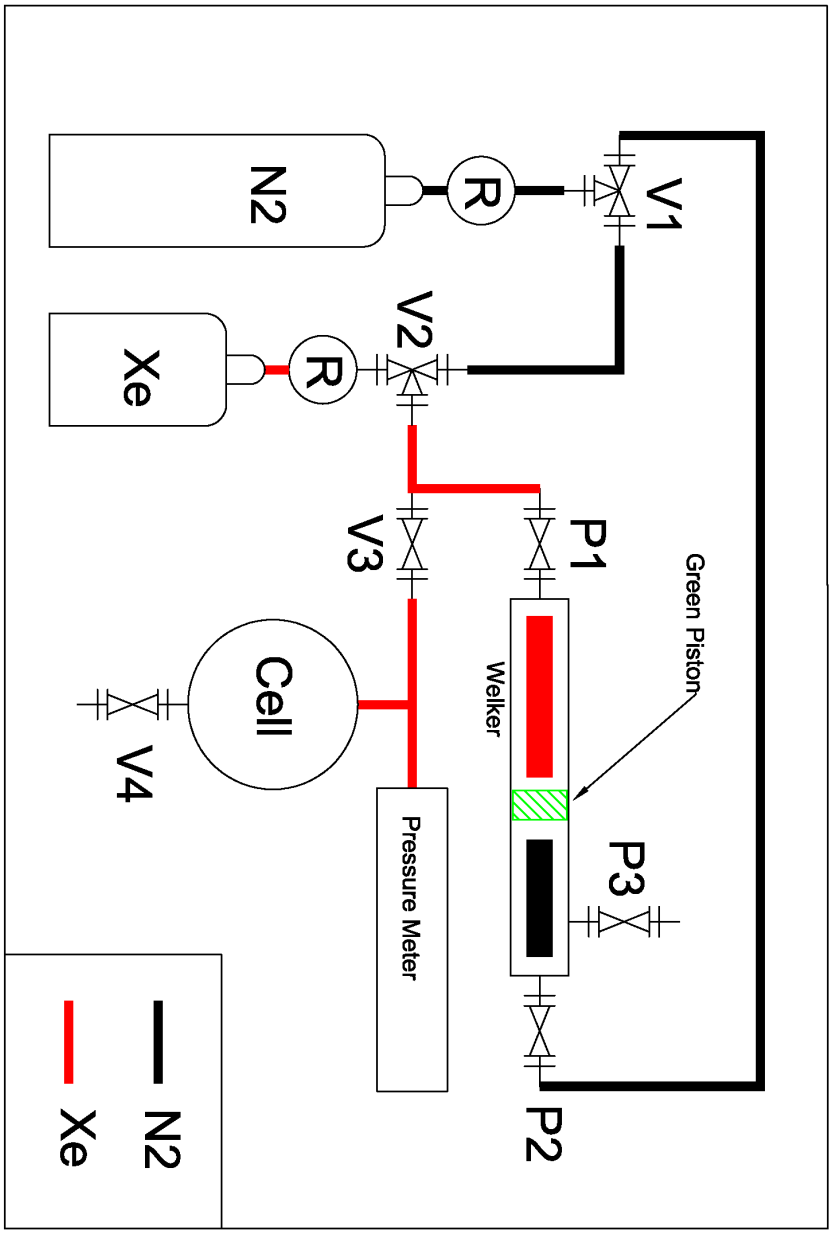

Figure B.1: Scheme of the pressure system used for the measurements in near-critical xenon. V1, V2, V3 and V4 are the gas valves; P1, P2 and P3 are the valves on the compression cylinder. Pressure chamber is labeled as "Cell"; "R" is the pressure regulator.

C

Comparison of calculated boiling temperature with experiments

We compare the theoretical value of the critical powers for the boiling as found in Fig.2.3 in Chapter 2 to the experimental critical powers found in Fig.3.2 of Chapter 3 and in Chapter 4. In Chapter 3, we find that the critical absorbed power for a particle with 40 nm radius (80 nm diameter) in water is 62.1 μW from Fig.2.3. This is calculated for a particle in water, but in our experiments we have particles in water on a silica substrate. To correct for this we use the average value of the thermal conductivity of water (0.65 $\mathrm{Wm^{-1}K^{-1}}$) and silica (1.38 $\mathrm{Wm^{-1}K^{-1}}$). Then we find:

$$P_{abs.}^{crit.} = \frac{\frac{1}{2}(0.65+1.38)}{0.65} \times 62.1(\mu W) = 97(\mu W) \tag{C.1}$$

Based on the diffraction-limited microscope's point spread function we estimate the size/diameter of the focus of the heating beam to be:

$$d = 1.22 \times \frac{\lambda}{N.A.} = 1.22 \times \frac{532}{1.45}(nm) = 448(nm) \tag{C.2}$$

Taking the refractive index of the medium surrounding a gold nanosphere to be the average of the refractive index of water and glass, we can use Mie theory to estimate the absorption cross section of the particle. We find $\sigma_{abs} = 1.7 \times 10^4$ $\mathrm{nm^2}$ at 532 nm. We can now relate the critical absorbed power for the formation of a nanobubble to the critical power *in the focus:*

$$P_{crit.}^{focus}\Big|_{80nm} = \left(\frac{A_{focus}}{\sigma_{abs}}\right) \times P_{abs.}^{crit.} = \left[\frac{\pi(448/2)^2}{1.7\times10^4}\right] \times 97(\mu W) = 0.9(mW) \tag{C.3}$$

This should be compared to critical powers measured in experiments, which depended on the conditions. For water on a BK7 glass substrate (Fig.3.6 in Chapter 3), the critical power was about 1.0 mW, in good agreement with the above estimate. On a fused silica substrate, because of the aberrations introduced by the poor index matching with the objective, the critical power rose to about 3 mW (see Fig.3.2, where the power is not corrected for objective transmission). A similar reduction of local intensity was found by Ruijgrok et al. [83] in the calculated and measured values of the intensity at the focus of a high numerical-aperture objective and attributed to spherical aberrations. For pentane on BK7 glass, the critical power was much lower, about 100 μW (Fig.3.5 in Chapter 3, insert).

In Chapter 4, we use a 50 nm diameter gold sphere in water and BK7 glass substrate. The critical absorbed power for the boiling in water around a 50 nm gold sphere is about 42.3 μW from Fig.2.3 in Chapter 2. If we consider the substrate, the critical absorbed power becomes:

$$P_{abs.}^{crit.}\Big|_{50nm} = \frac{\frac{1}{2}(0.65+1.11)}{0.65} \times 42.3(\mu W) = 57.3(\mu W) \tag{C.4}$$

The N.A. of the objective used in Chapter 4 is 1.4, so the diffraction-limited diameter of the focus of the CW heating beam (532 nm) is:

$$d = 1.22 \times \frac{\lambda}{N.A.} = 1.22 \times \frac{532}{1.4}(nm) = 464(nm) \tag{C.5}$$

The absorption cross section of a 50 nm diameter gold sphere on a BK7 substrate in water, taking into account the BK7 substrate, is calculated to be about 7650 nm^2 at 532 nm. Using the same equation as Eq.C.3, we find the critical power *in the focus* for the formation of a vapor nanobubble around a 50 nm gold sphere:

$$P_{crit.}^{focus}\Big|_{50nm} = \left(\frac{A_{focus}}{\sigma_{abs}}\right) \times P_{abs.}^{crit.}\Big|_{50nm} = \left[\frac{\pi(464/2)^2}{7646}\right] \times 57.3(\mu W) = 1.3(mW) \tag{C.6}$$

The critical power found in such calculations is close to, but a bit higher than the CW heating power found in our pump-probe experiments when the vapor bubble forms. Note that in the pump-probe experiments, both the pump and probe pulses contribute to the temperature rise of gold nanoparticle. More importantly, the acoustic vibration of the gold nanoparticle can behave as a trigger to tear the hot liquid molecules apart and initiate a vapor bubble.

D

Energies involved in the vapor bubble growth

To understand bubble growth and instability better, we have estimated the main energy contributions involved in the explosion. Although this process appears to follow an inertial regime, we neglected kinetic energy, which can be considered in a future dynamic model. The three main contributions mentioned in the main text of Chapter 3 were calculated as follows, assuming the non-evaporated overheated liquid is pushed mechanically by the created vapor, without heat conduction through the interfaces:

i) Surface energy: it is calculated for varying bubble radius from the surface tension which is temperature dependent. The temperature is assumed to be the equilibrium one, although this is certainly not true during the expansion.

ii) Latent heat and heat capacity: this energy is calculated from the internal energy of liquid and gas, as a function of bubble diameter.

iii) Overheated liquid thermal energy: this is the heat stored in the overheated layer, integrating all layers of liquid whose temperature exceeds the equilibrium curve between regimes I and II (dashed line in Figure D.1). The temperature profiles of the liquid immediately before the explosion (blue solid curve) and for two different bubble diameters (red curves) are presented in Fig.D.1. Liquid layers with temperature above the dashed curve are in principle able to give energy to the vapor shell and to feed the expansion.

The three energy contributions above are plotted as functions of the bubble radius in Fig.D.2. Only half of the overheated liquid energy has been used to heat the bubble, the other half was assumed to dissipate into the colder outer layers. The net energy contribution, plotted in Fig.D.3 against bubble radius, is

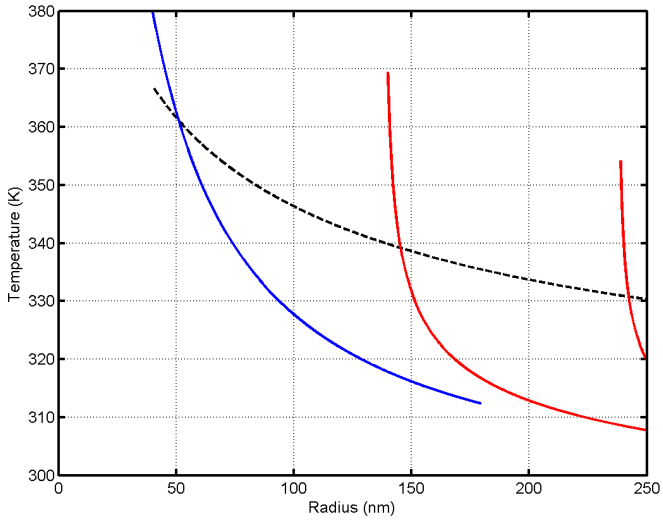

Figure D.1: Temperature profiles along the radial direction. The solid blue curve shows the initial temperature profile. The dashed black curve (phase diagram) gives the surface temperature of the vapor shell as found from the Laplace pressure. The solid blue curve crosses the dashed black curve at a radius of about 50 nm, corresponding to an overheated liquid between 40 nm and 50 nm. The solid red curves show the temperature of the liquid after it has been pushed out by the vapor shell. The part of the solid red curves above the black dashed curve at the vapor shell radius (i.e. the start of the red curves) represents excess energy partly available to feed the explosion.

negative for small radius, driving bubble expansion. Its slope, corresponding to the driving force, changes sign for 150 nm, creating an effective potential resisting expansion. In the absence of friction and heat diffusion, the maximum bubble diameter would be 230 nm. However, dissipation soon cools the surface bubble and suppresses overheating, entailing the collapse of the bubble until heating by the nanoparticle can start a new explosion.

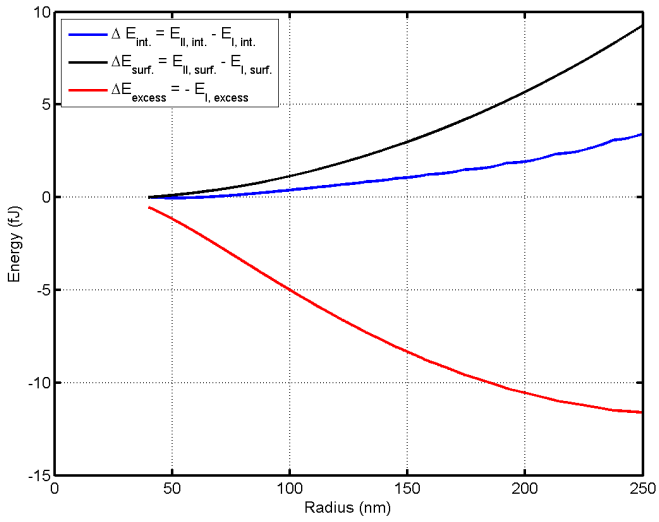

Figure D.2: Variations in internal energy (blue curve), surface energy (black curve) between state I and state II, and excess overheating energy (red curve; only half this energy is available for the bubble heating, the rest is assumed to diffuse to the cold outside liquid layers).

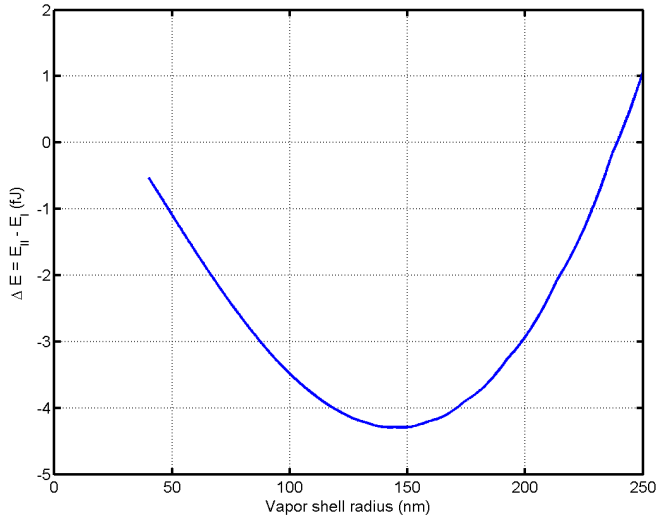

Figure D.3: The energy difference between state I and state II as a function of vapor shell radius. In principle there is enough excess energy to expand the vapor shell up to about 240 nm radius, much beyond the steady state radius of about 50 nm.

E

Analysis of delay time between two successive explosions

In order to understand the details of the delay time between two successive explosions in Chapter 3, we plot the delay time as a function of event number (red dots) as well as a histogram of the delay times (green histogram) in Fig.E.1. We attribute the strong correlation between successive delay times observed in these plots to the slow drift of the laser power, during which bubbles appeared, maintained a high repetition rate, and eventually subsided (blue trace in insert). Indeed, upon selecting a part of the data from n=800 to 2600 where laser power drift appears negligible, the data shows essentially no correlation between successive delay times. We fit the histogram of the selected delay times from n=800 to 2600 with a Gaussian distribution function as follows:

$$p(\tau) = \frac{A}{\omega\sqrt{\pi/2}} exp\left[-\frac{2(\tau-\tau_c)^2}{\omega^2}\right] \tag{E.1}$$

The fitted results are shown in Fig.3.3 (d) in Chapter 3.

To further illustrate the absence of correlation between successive delay times we simulated random delay times using the fitted Gaussian distribution. We created scatter plots of successive delay times for both the experimental data and simulation (in which correlation is absent), see Fig.E.2. By comparing the two scatter plots, we conclude that the delay time data in the central part of Fig.E.1, which we think is governed solely by the nanobubble system and not by drift of the laser power, is essentially uncorrelated.

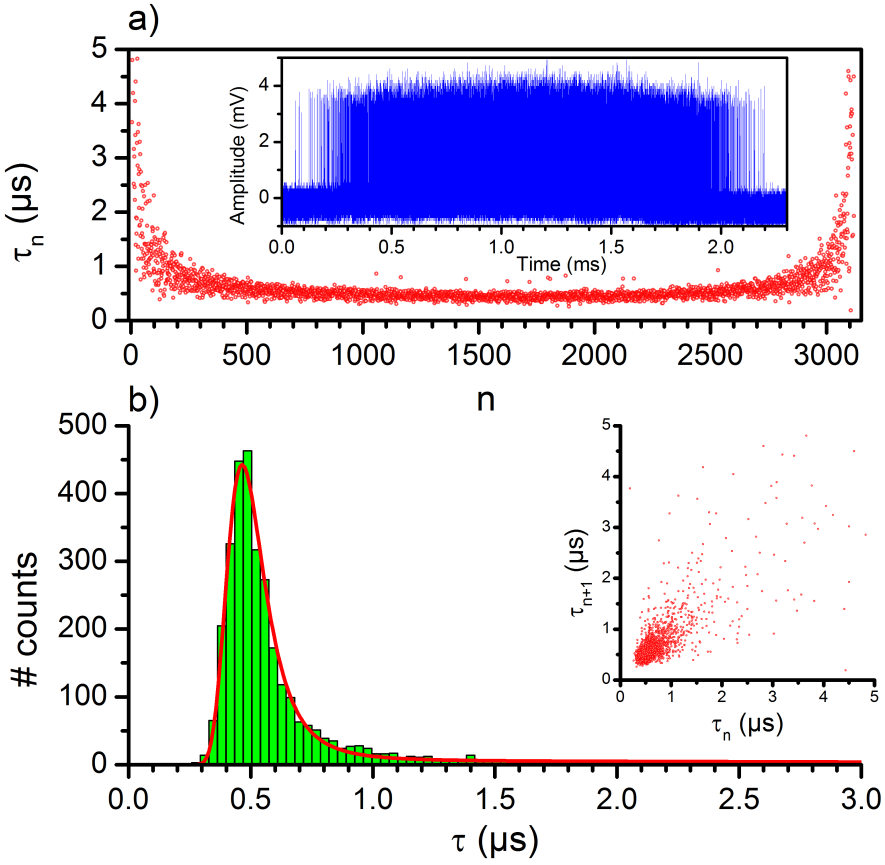

Figure E.1: a) The delay time between two successive explosions as a function of the event number n. Insert: time trace of the intensity of the scattered probe light; b) Histogram of the delay time distribution. The red line is a fitted curve. Insert: the scatter plot of τ_{n+1} and τ_n.

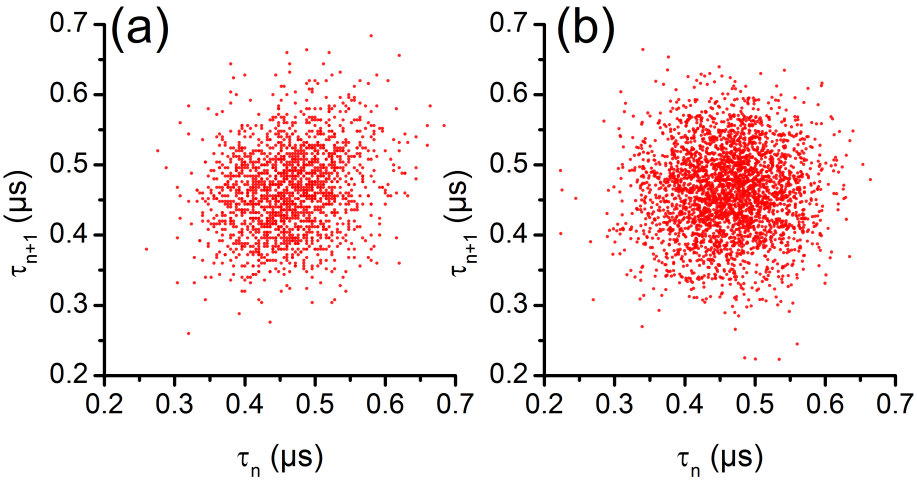

Figure E.2: a) A scatter plot of τ_{n+1} and τ_n using the experimental data; b) A scatter plot of simulation of a random succession of delay times drawn from the Gaussian distribution that is used to fit to the data from n=800 to 2600.

F

Triggering a second explosion by a sound wave

Hereafter, we briefly speculate about the mechanism of after-burst triggering by the echo. If enough energy is left in the hot liquid and in the gold nanoparticle after the first explosion, and if the returning cooled water has enough contact time with the nanoparticle to become overheated again, the system may be reloaded for a new explosion, although the temperature profile is much less extended than that before the main explosion. The heat diffusion length for a time of 150 ns, the time interval between the main bubble collapse and the arrival of the echo, is 100 nm ($D_{pentane} = 6 \times 10^{-8}$ m^2/s). For a 1 μs time it's about 2.5 times larger, 250 nm. For a long enough waiting time, a second explosion can take place, with a reduced amplitude as there is less energy stored in the overheated water to feed the expanding after-bubble. Sometimes, we even observe a third after-burst, which appears again 150 ns after the second one (see Figure F.1). This delay of 150 ns corresponds to twice the propagation time in the oil gap ($2 \times 100 \mu$m at 1350 m/s). Indeed, the first echo from the far side of the coverslip arrives 60 ns after the explosion, while the bubble just contracted and not enough energy has been transferred to the liquid yet. The echo from the objective surface arrives 150 ns later still (see Fig.3.4.c in Chapter 3) and finds enough hot water to trigger a second explosion or after-burst. In some conditions two or more afterbursts can be observed (see Fig.F.1). In these events, the nanobubble performs as an amplifier fed back on itself, producing damped relaxation oscillations. A similar phenomenon observed in water is shown in Chapter 3. However, in this latter case, the oscillation period is about 30 ns and is too short to arise from an acoustic echo. We attribute this instability to bub-

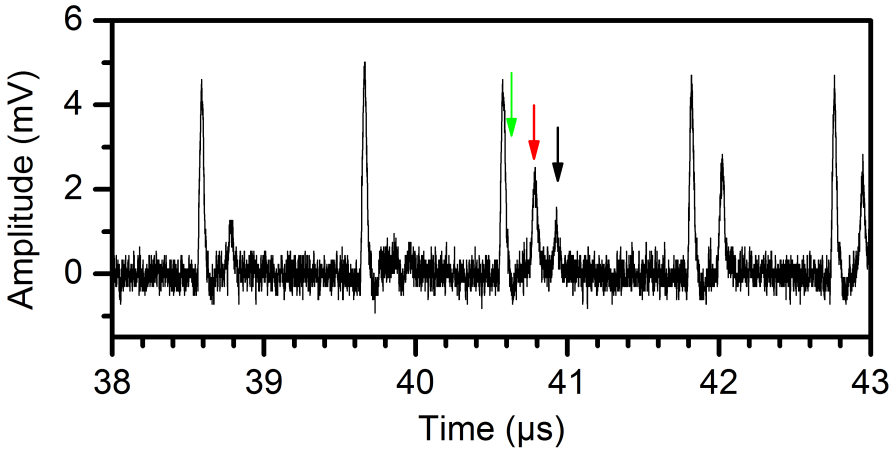

Figure F.1: The time trace including a third after-burst (black arrow). The experimental conditions are the same as Fig.3.4 in Chapter 3. The gold nanoparticle is immersed in n-pentane.

ble dynamics itself. These observations highlight the remarkable sensitivity of the nanobubble to extremely weak multiple acoustic reflections from interfaces more than 100 μm away.

G

Single-shot time trace of a persistent nanobubble

In Fig.G.1, we present a single-shot time trace of the signal of a nanobubble formed by raising the heating power above the critical value. This event is a typical one taken out of the long time trace with hundreds of explosions, shown together with the heating intensity profile. The bubble starts with a small explosion clearly visible in Fig.G.1.a, and is followed by a persistent phase before disappearing about a microsecond later when the power is decreased again. The histogram of Fig.G.1 (c) shows the jitter delays Δ between the heating pulse and the time of the explosion, taken at the mid-rising edge of the explosion signal. These delays are all positive, confirming that the explosions are all caused by the heating increase. Moreover, we see that the histogram is almost 0.5 μs broad, comparable to the spread of inter-explosion delays in the time traces in Chapter 3 with constant heating.

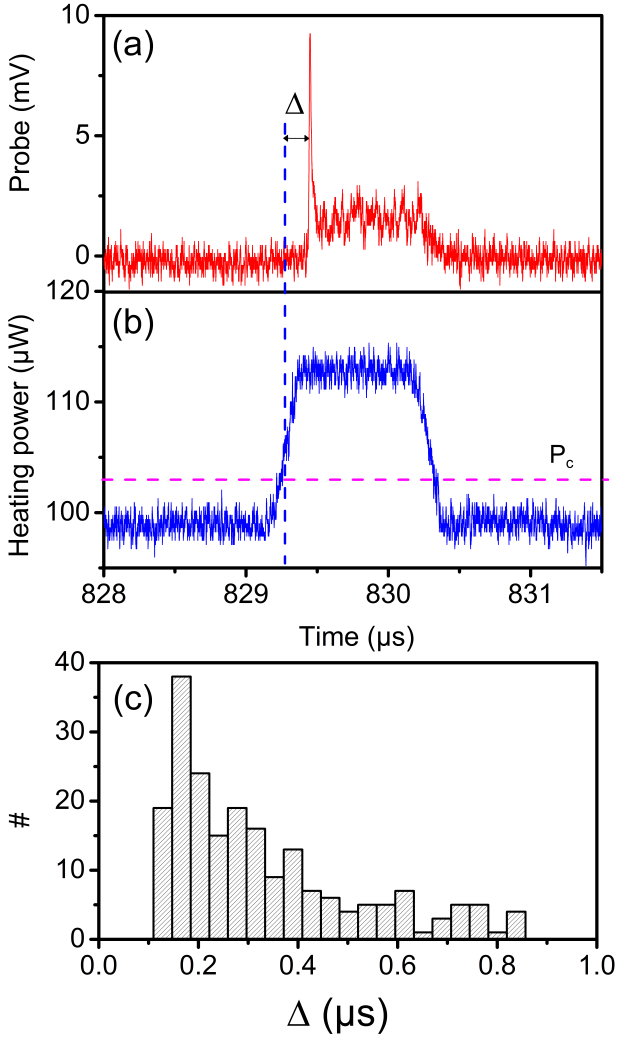

Figure G.1: The non-averaged time trace showing the improvement of nanobubble stability. a) Probe signal; b) Heating power; The heating beam is modulated by AOM, using a block pulse profile with a frequency of 100 kHz, and a duty cycle of 10% (1 μs on-time in a 10 μs period); c) The histogram of the jitter delay between the probe rise edge and heating rise edge. The gold nanoparticle is immersed in n-pentane in these measurements.